

**Coupled Computational Fluid Dynamics and MOC Neutronic Simulations of  
Westinghouse PWR Fuel Assemblies with Grid Spacers**  
**Jin Yan<sup>1</sup>, Brendan Kochunas<sup>2</sup>, Mathieu Hursin<sup>2</sup>,  
Thomas Downar<sup>2</sup>, Zeses Karoutas<sup>1</sup>, Emilio Baglietto<sup>3</sup>**

<sup>1</sup>Westinghouse Electric Company LLC, Columbia, SC, USA

<sup>2</sup>University of Michigan, Ann Arbor, Michigan

<sup>3</sup>CD-adapco, Melville, New York

[yan3j@westinghouse.com](mailto:yan3j@westinghouse.com)

**Abstract**

Neutronic coupling with Computational Fluid Dynamics (CFD) has been under development within the US DOE sponsored “Nuclear Simulation Hub”. The method of characteristics (MOC) neutronics code DeCART ([Joo, 2004], [Kochunas, 2009]) under development at the University of Michigan was coupled with the CFD code STAR-CCM+ to achieve more accurate predictions of fuel assembly performance. At Westinghouse, lower order, neutronic codes such as the nodal code ANC have been coupled to thermal-hydraulics codes such the subchannel code VIPRE to predict the heat flux and fuel nuclear behavior. However, a more detailed neutronics and temperature / fluid field simulation of fuel assembly models which includes explicit representation of spacer grids would considerably improve the design and assessment of new fuel assembly designs. Coupled STAR-CCM+ / DeCART calculations have been performed for various representative three-dimensional models with explicit representation of spacer grids with mixing vanes. The high fidelity results have been compared to lower order simulations. The coupled CFD/MOC solution has provided a more truthful model which includes a more accurate representation of all the important physics such as fission energy, heat convection, heat conduction, and turbulence. Of particular significance is the ability to assess the effects of the mixing grid on the coolant temperature and density distribution using coupled thermal/fluids and neutronic solutions. A more precise cladding temperature can be derived by this approach which will also enable more accurate prediction of departure from nucleate boiling (DNB), as well as a better understanding of DNB margin and crud build up on the fuel rod.

**Keywords:** Neutronic, Thermal hydraulics, CFD, code development, code coupling, etc.

**1. Introduction**

DOE’s Consortium for Advanced Simulation of Light Water Reactors (CASL), based at Oak Ridge National Laboratory (ORNL), is partly designed to build models that will help utilities optimize the performance of existing reactors. This paper summarizes the collaborative effort by the University of Michigan, Westinghouse Electric Company (WEC), CD-adapco, and ORNL to complete the research project, “Apply a baseline transport (DeCART) and CFD (STAR-CCM+) capability with loose coupling to a PWR 3x3 fuel pin with a spacer grid to demonstrate feedback coupling” in the Advanced Modeling Applications (AMA) Focus Area (FA) of CASL. This work leverages the ideas and methods from previous work by the authors described in [Weber, 2007] and [Sofu, 2007],

however it differs from the previous work by using a different CFD code and consequently the mechanics of the coupling. The analysis performed here also involves the explicit modeling of a WEC grid spacer, which to the best of the authors' knowledge has not been done previously. The following paper will first describe the methodology developed to couple DeCART and STAR-CCM+ and the verification and validation performed on the coupled codes. The paper will then describe the application to the 3x3 fuel pin with an explicit grid model.

## 2. Neutronic and CFD Coupling Methodology Development

### 2.1 Coupling Approach

The coupling of DeCART with STAR-CCM+ is based on file input / output. All data shared between DeCART and STAR-CCM+ are written to the files on the hard disk in the working directory. Both DeCART and STAR-CCM+ are run sequentially to completion. A criterion is set by the user to determine the convergence of both DeCART and STAR-CCM+. Typically, it is based on the fission source convergence on the DeCART side and on the energy residual on the STAR-CCM+ side. One iteration of a coupled calculation is composed of a completed DeCART and STAR-CCM+ run. Core averaged quantities (multiplication coefficient, fuel averaged temperature) are monitored at each iteration and the calculation is stopped when those quantities reach their asymptotic value. By default the number of iterations is set to 10 but it can be modified by the user.

At each iteration, the following information is passed between DeCART and STAR-CCM+:

- Enthalpy source [W/m<sup>3</sup>] provided by DeCART and read by STAR-CCM+
- Temperature [K] & water density [g/cm<sup>3</sup>] provided by STAR-CCM+ and read by DeCART.

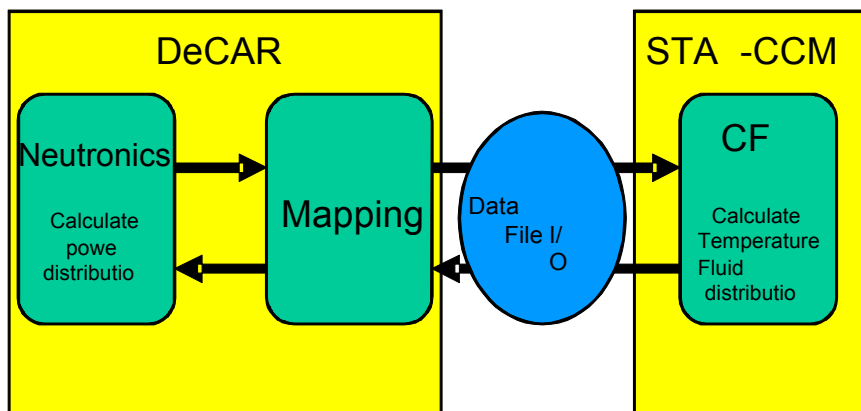


Figure 1 - Neutronic & CFD coupling mechanism

Due to the different spatial discretization used by the neutronic and the CFD codes, a mapping between DeCART and STAR-CCM+ is necessary. Initially, the position of the STAR-CCM+ cell centroid coordinates are provided by STAR-CCM+ to DeCART to setup the mapping between STAR-CCM+ and DeCART mesh. The mapping is addressed in more detail in the next section. The guideline for the coupling is to allow STAR-CCM+ to be treated as a “black box”, and for DeCART to manage the data. Therefore, the data files are written in a manner to simplify the task for the CFD code. Each line of the file contains data for one CFD cell.

## 2.2 Importing/Exporting Data from STAR-CCM+

STAR-CCM+ provides various ways to import / export cell wise data. One of the most straightforward ways is to take advantage of the so called (x,y,z) tables to extract the geometric information together with the temperature and density. The enthalpy sources are imported through tables as well. Another method is via user subroutines. The initial use of the (x,y,z) table was motivated by their convenience. While the main drawback is the time penalty taken at each iteration by the two codes to read and write the necessary data. Additionally, this approach puts a higher requirement on computational resources somewhat limiting the size of problems. In the long run, user subroutines will be developed to handle all the data exchanges between DeCART and STAR-CCM+.

## 2.3 Mesh Mapping Strategy

Since the neutronic and thermal hydraulic codes use different spatial discretization, a mapping between DeCART and STAR-CCM+ is necessary. An example of the respective DeCART and STAR-CCM+ mesh can be seen in the Figure. Presently, only conformal material meshes are allowed: STAR-CCM+ material boundaries must be inline with the DeCART material boundary. It should be noted that Figure illustrates a more strict mesh conformance between DeCART and STAR-CCM+ where the DeCART mesh boundaries coincide with mesh boundaries in STAR-CCM+. This level of mesh conformance is not normally required. The mesh within a material region can then be unstructured, as long as the STAR-CCM+ is finer than the DeCART mesh. The STAR-CCM+ mesh are assigned based on the position of their centroid. Each STAR-CCM+ cell is assigned to the DeCART uniform cross section region in which the centroid lies.

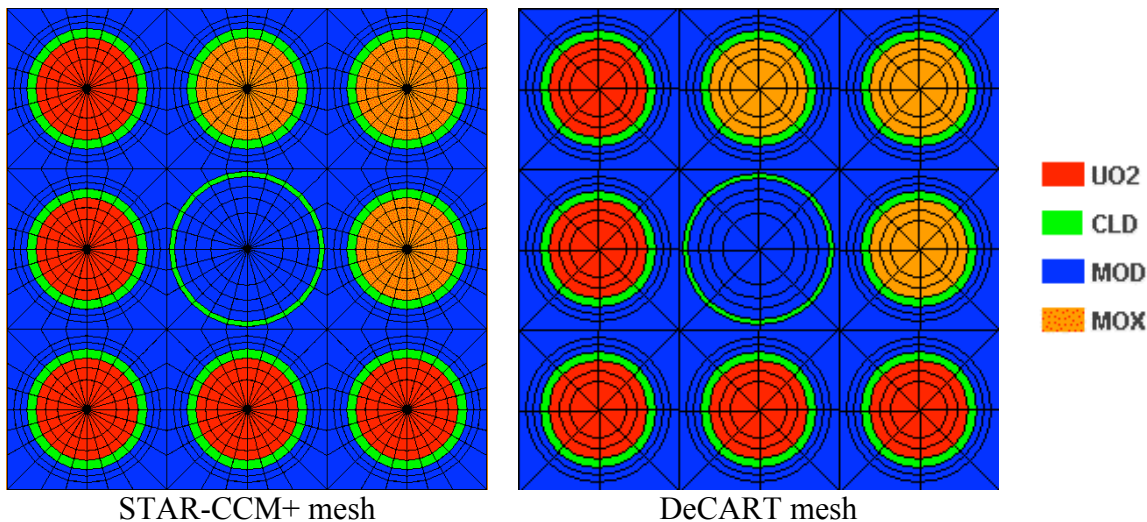


Figure 2 - Star-CCM+ and DeCART spatial discretizations.

To deal with the situation that the meshes in DeCART and STAR-CCM+ have different origins, DeCART is provided with the coordinates of its origin in the STAR-CCM+ system of coordinates. The origin of the DeCART coordinate system is always in the northwest (or upper-left) corner of the x-y plane and axially at the bottom of the problem domain. The variables  $x\_shift$ ,  $y\_shift$ , and  $z\_shift$  are the coordinates of the DeCART origin in the STAR-CCM+ coordinate system in centimeters are required by the DeCART input. The other modification to both DeCART and STAR-CCM+ are described in the next section.

## 2.4 Input Files Modification for Coupling

The present section described the modification to be made to the DeCART and STAR-CCM+ input in order to run a coupled case.

### 2.4.1 DeCART Input

In order to properly setup DeCART for coupled calculation, 3 modifications to the input deck must be done. All three concern the OPTION block.

- Card **feedback**;  
1 logical (use of internal T/H solver)  
Turn internal thermal hydraulic feedback off.
- Card **read\_th**;  
3 logicals (read T/H, axial reflector presence, print power).  
Turn on the reader of T/H feedbacks and the writer of power source.
- Card **star\_opt**;  
1 logical (read STAR-CCM+ / STAR-CCM+ data)  
3 real (x,y,z)., Coordinates of the DeCART origin in the STAR-CCM+ laboratory coordinates system.

### 2.4.2 STAR-CCM+ input.

The setup of the STAR-CCM+ model to be coupled is automatized through a java routine. The java routine creates 3 tables necessary for the coupling and provides STAR-CCM+ with their locations:

- **indec**; writes `cfgeom_0001.cpl`
- **th**; writes `cfdata_0001_1.cpl`
- **power**; reads `power_p0001.cpl`

Then, the routine turns on the energy source term option in the fuel pellet regions and links the power table to the enthalpy source in those regions. The java subroutine needs to be run only once in the lifetime of a STAR-CCM+ model.

## 2.5 Running a coupled calculation

The present section is dedicated to running coupled DeCART STAR-CCM+ cases. The coupled calculation is driven by STAR-CCM+ through the java macro “directcpl.java”.

The first step is to put all the necessary components in the same directory:

- STAR-CCM+ sim file
- Java subroutine: `directcpl.java`
- DeCART executable (`decart-v2.exe`)
- DeCART input deck

The subroutine `directcpl.java` assumes that the various tables needed for the coupling are already available in the STAR-CCM+ sim file. `directcpl.java` performs the following tasks:

1. Clear/Initialize STAR-CCM+ solution

2. Extract information for the indices table and writes the `cfd_geom_0001.cpl` file
3. Extract initial information for the th table and writes the `cfd_thdata_0001_1.cpl` file
4. Call DeCART through a system command call. Run DeCART to completion (user defined convergence criterion).
5. Initialize STAR-CCM+ solution
6. Import `power_p0001.cpl` file in the power table
7. Run STAR-CCM+ to completion (user defined convergence criterion).
8. Extract initial information for the th table and writes the `cfd_thdata_0001_1.cpl` file
9. Go back to step 4 and repeat 10 times.

By default 10 fixed point iterations are assumed to be enough to obtain a converged coupled solution. This number can be changed by the user to continue the coupled calculation passed 10 iterations if the convergence behavior is slow or to stop it earlier, if convergence is observed earlier.

### 3. Neutronic and CFD Coupling of 3X3 fuel with one real grid spacer

The Vantage 5 Hybrid (V5H) fuel assembly is a fuel design which has been used in Westinghouse PWR plants in the past. Since many advanced nuclear fuel thermal hydraulic research has been performed using this design [5-7], it was decided that V5H design would be provided to the CASL project for advanced model development. The goal is to have a multi-physics model, which includes the effect of Neutronic, Thermal Hydraulic, Structure, Corrosion, Pellet Cladding Interaction (PCI), Crud and GTRF, developed based on the 3x3 V5H design. The 3X3 pin V5H axial and radial geometry details are depicted in Fig 3 and Fig 4. It contains one V5H mid-grid with all the strap, vanes, dimples, and springs. The model has one grid span of fuel rod, and fuel pellets. The model was provided to CASL so test problems can be established and executed for the key challenge problems: crud, corrosion, PCI, fuel performance GTRF, etc. New models can also be developed and compared to available data for validation. The first stage of the multi-physics model development is the Neutronic & CFD coupling.

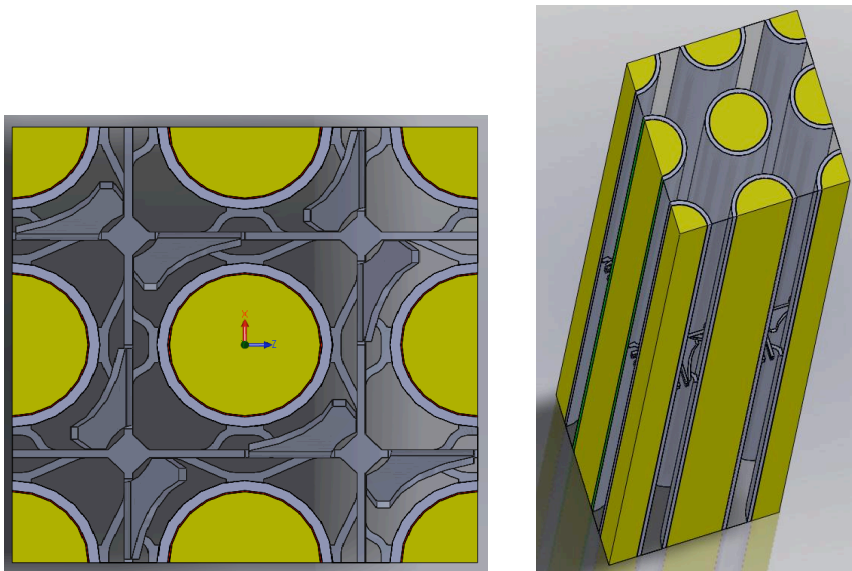


**Figure 3 –3X3 pin V5H solid model**

The objectives of the Neutronic & CFD coupled modeling of 3X3 pin V5H fuel are: (1) to demonstrate the effect of the coupling Neutronic and CFD; (2) to demonstrate the ability of the method in predicting

the key flow features induced by the mixing vane; (3) to illustrate the effect of the mixing vaned grid on the heat transfer.

### 3.1 CFD model of 3X3 fuel with one real grid spacer

There are seven V5H mid-grids in the model. Six of the 7 spacer grids are simply represented by momentum sinks in the flow, while one of the grids is explicitly represented. This explicit grid is located at grid 5 position with an elevation of 2180mm as shown in Fig.4.

#### 3.1.1 Computational Domain and Mesh

The fuel pellets are modelled as one continuous solid domain with the appropriate material properties. The cladding and grid are modelled as separate solid domains with the appropriate material properties. The coolant is sub-cooled water and the water properties were obtained from the National Institute of Standards and Technology (NIST) data base. The mesh consists of 37.5M hexahedral cells with adequate amount of cells to resolve the grid thickness based on extensive validation work performed in Westinghouse [7-9].

#### 3.1.2 Physics Model, Material Properties and Boundary Conditions

Two CFD models have been developed: One with coupled neutronics and the other using an averaged energy source term in the fuel pellet solid to represent a flat, uniform fission energy source term. The boundary conditions of the CFD models are the same as the core conditions in a real plant, and are listed in Table 1 together with the main CFD model settings.

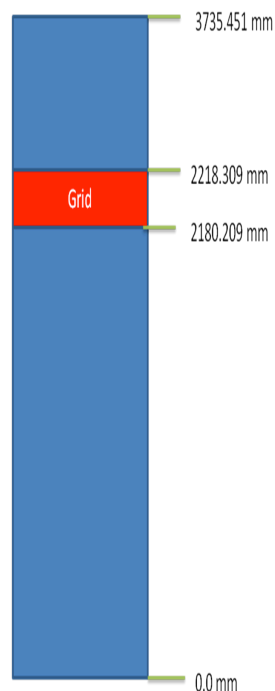


Figure 4 – CFD domain

**Table 1 – Boundary Conditions for 3x3 CFD Model**

<b>Turbulence Model</b>	<b>Realizable k-ε turbulence model with all y+ wall treatment [10]</b>
<b>Solid surfaces (sides)</b>	<b>Symmetry</b>
<b>Solid surfaces (rest)</b>	<b>wall</b>
<b>Volumetric heating of the pellet pins</b>	<b>Averaged power: 3.931E8 W/m<sup>3</sup> Coupled case: Calculated by DeCART</b>
<b>Fluid inlet</b>	<b>velocity inlet at 4.951298m/s and 583.7K</b>
<b>Fluid outlet</b>	<b>Pressure outlet</b>
<b>Fluid side surfaces</b>	<b>Periodic</b>
<b>Reference pressure</b>	<b>2250 psi</b>

### 3.2 DeCART model of 3X3 fuel with one real grid spacer

The computational domain of the DeCART model is exactly the same as the CFD domain. The neutronics mesh used for this problem is shown in the Fig.5 below.

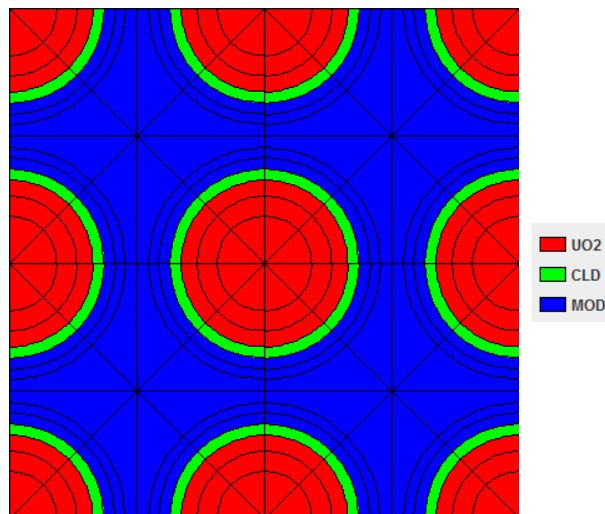


Figure 5 – DeCART Mesh

Axially, the problem was divided into 21 segments. Ten segments below the grid spacer, ten above the grid spacer, and one for the grid spacer. The one axial segment for the grid spacer was sized at 8.81 cm, which is 5 cm taller than the grid spacer itself. This modelling approximation was introduced because the 2-D/1-D method employed by DeCART is limited in its ability to handle very small axial mesh. DeCART's current geometry representation is not robust enough to explicitly model the grid spacer structure, so it was homogenized with the coolant within the given axial segment where the total mass of the grid spacer and coolant are preserved. This modelling approximation will introduce some error. It should also be noted that in the neutronic model the fluid density is not mapped to the homogenized

grid-spacer/coolant region, it is however still applied to the fuel and clad within this axial segment. The total number of spatial mesh regions in DeCART was 4704. The problem was executed in parallel on 21 processors each requiring about 40MB of memory. On average, the total time DeCART took to run one coupled iteration was ~50 min. However, approximately only ~3 min. of the total run time per coupled iteration was spent solving the neutronics problem; the rest of the time was for the file I/O data transfer operations.

Typical zircaloy materials are assumed for the cladding material and the fuel is assumed to be fresh UO<sub>2</sub> enriched to 5wt% U-235 and loaded uniformly. Reflective boundary conditions are applied for the radial direction and vacuum boundary conditions for the axial directions. This means the radial relative pin power distribution will be the same for all the pins. So, the neutronic heat source is only providing an intra-pin power shape and axial power shape to STAR-CCM+.

### 3.3 DeCART Results

The axial power shape predicted by DeCART is shown in Fig.6. The radial power distribution is shown for the plane with the grid spacer and the peak plane in Fig. 7. The temperature distributions mapped to DeCART are similarly shown for these planes in Fig.8 respectively. Here we note that the axial power shape varies much more significantly than the intra-pin power shape. We also note that the axial power shape is arguably a little more bottom peaked than what is typically observed in at operating conditions in a PWR, and this is likely attributed to the test problem definition which includes only fresh fuel and reflective boundary conditions in the radial direction. The bottom peaked axial power is driven primarily by the moderator density distribution axially. So, one should not expect the typical axial power shape of a PWR core since this is largely determined by the exposure distribution of the assemblies in the core and the presence of fission product poisons. This should not detract from any of the conclusions drawn from the results here since the comparison is between a flat average result and a result with a shape.

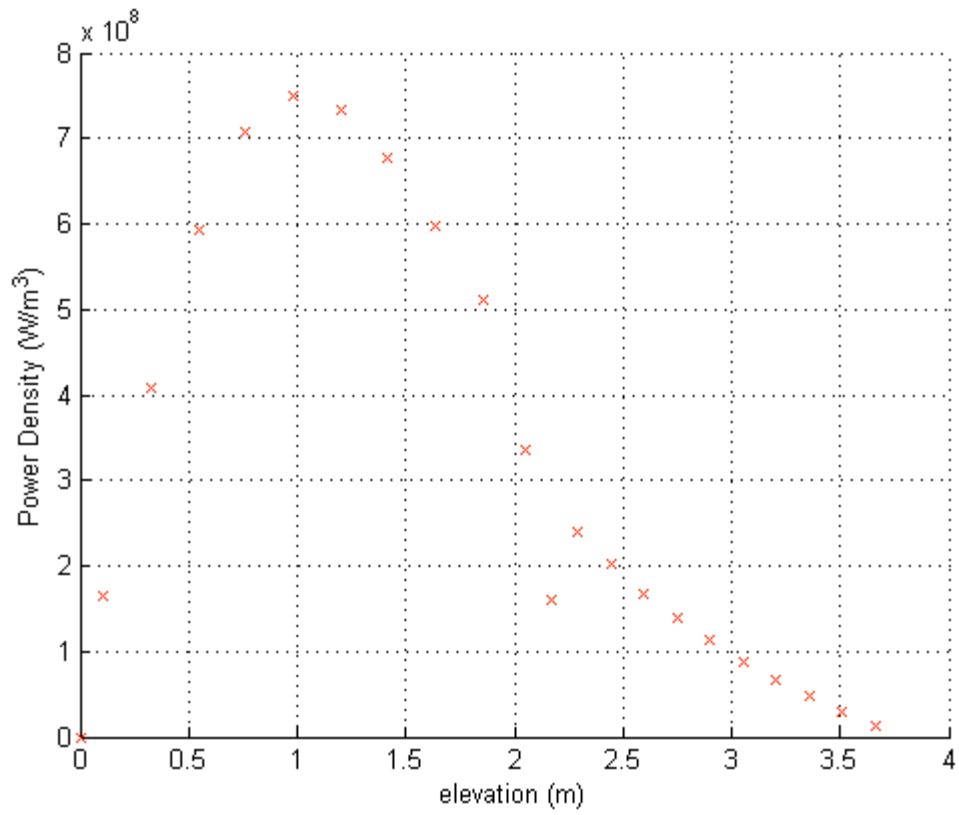


Figure 6 - Axial Relative Power Shape

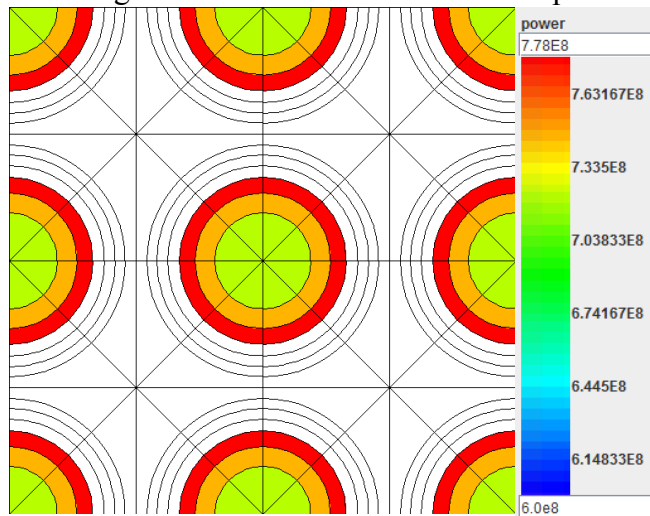


Figure 7a - DeCART power distribution (W/m<sup>3</sup>) at peak plane

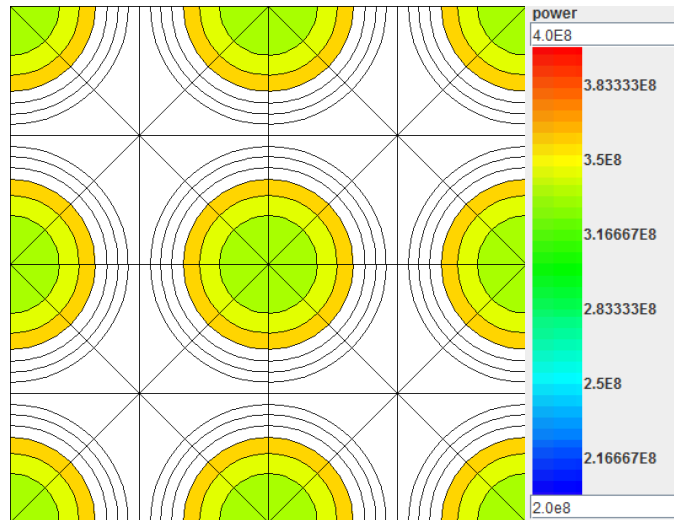


Figure 7b - DeCART power distribution ( $W/m^3$ ) at grid spacer plane

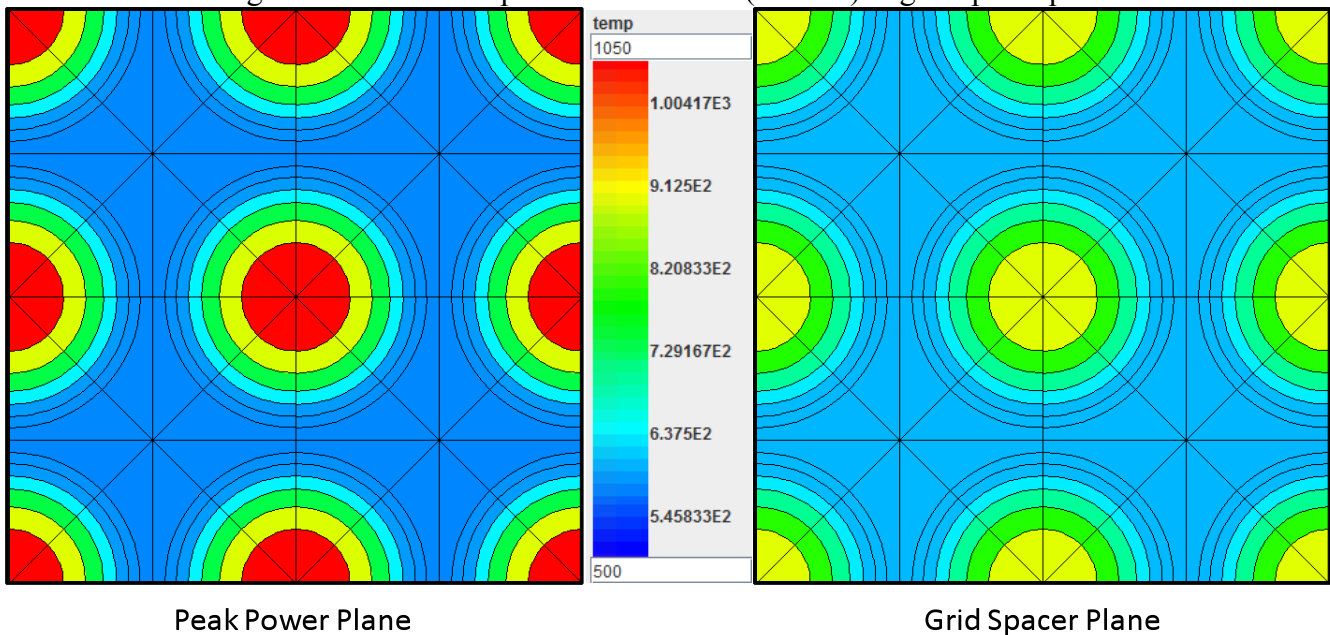


Figure 8 - DeCART temperature distributions (Kelvin)

### 3.4 CFD results

The CFD modelling approach adopted in this work is consistent with the guidelines developed and adopted by Westinghouse Nuclear Fuel [7-9]. In particular the previous work has provided guidelines on the grid quality, discretization methods and numerical practices to adopt, and have further demonstrated the applicability of single phase flow CFD to accurately predict flow field as well as heat transfer characteristics inside fuel bundle.

In the present work a 3x3 rods domain is adopted in order to reduce the computational requirements during the development phase and further given the operational conditions simulated it is not possible to produce an exact validation against available experimental data, nevertheless a qualitative discussion can be provided in comparison with test on a 5x5 model at a lower Reynolds number.

Fig.9 represents the experimental secondary velocity measurements for the case of a 5x5 spacer at locations respectively 17, 33 and 50 mm downstream of the grid spacer. The velocity measurements are presented for 4 different sub-channels to showing the noticeable difference related to finite geometry and the presence of the surrounding test shroud. If we compare Fig.10, which presents the results of the present calculations for an infinite array of rods we can notice some clear differences but also certain important commonalities. The presence of mixing vanes generates 2 main vortices in the sub-channel, which have around 45 degrees rotation from the underlying rods distribution, while in the computations at the 17 mm locations these 2 vortices do not show such rotation, which is instead noticeable at higher locations (33 and 50 mm). Furthermore at the 17mm location both experiments and CFD capture the presence of a smaller secondary vortex in the tight gap region. Trying to judge the causes of the difference at the 17 mm location, clearly the higher flow velocity seem the most probable cause as the rotation is delayed further downstream.

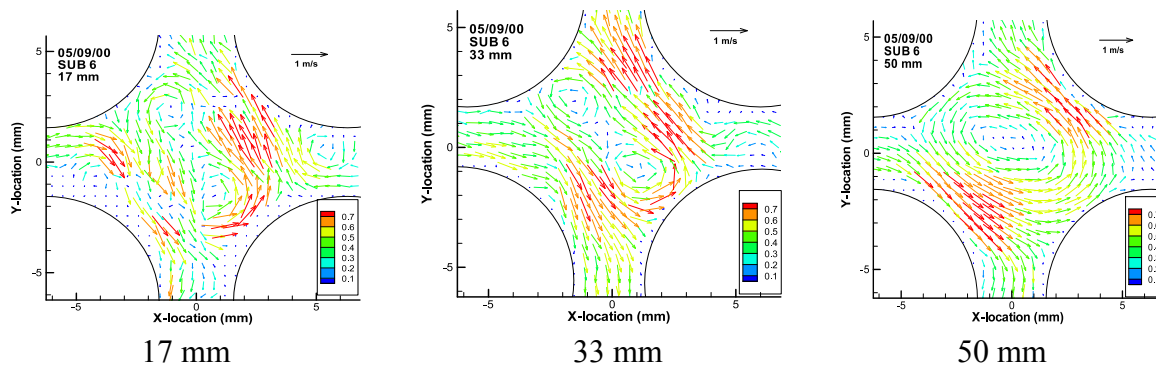


Figure 9 - (Test data) Time-averaged flow fields at axial location of 17, 33, and 50 mm at a mean velocity of 2.4 m/s (8 ft/s).

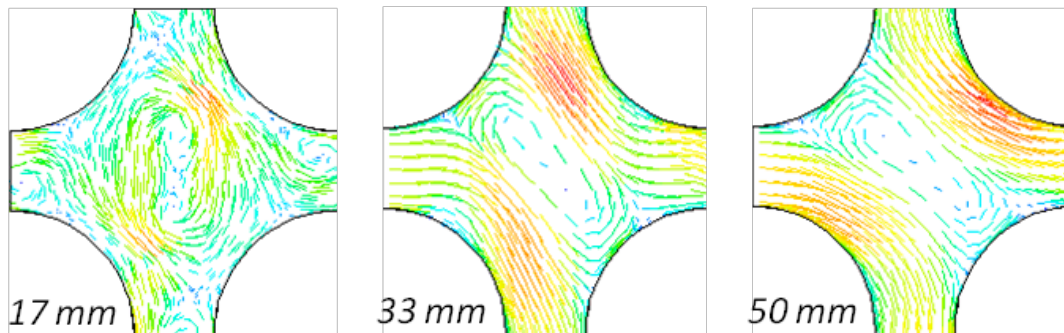


Figure 10 - (CFD results) Time-averaged Flow Fields for at an Axial Location of 17, 33 and 50 mm and a Mean Velocity of 5.35 m/s.

### 3.4.1 Averaged Power (Decoupled) Modelling Results

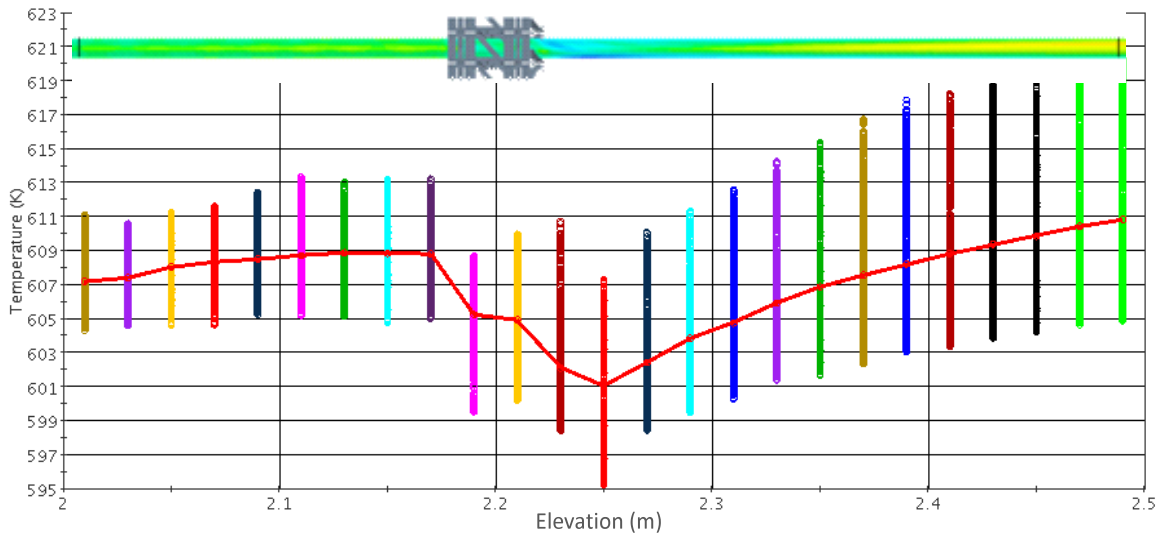


Figure 11 - Temperature distribution near the spacer grid on the central fuel rod (decoupled)

Fig.11 shows the average (red line) and local Temperature distribution along the rod, before and after the spacer grid. Very interestingly, we can not only see the average trend but also the local temperature non-uniformity. The temperature scene clearly shows the temperature decrease after the spacer and the non-uniformity of the temperatures around the rod.

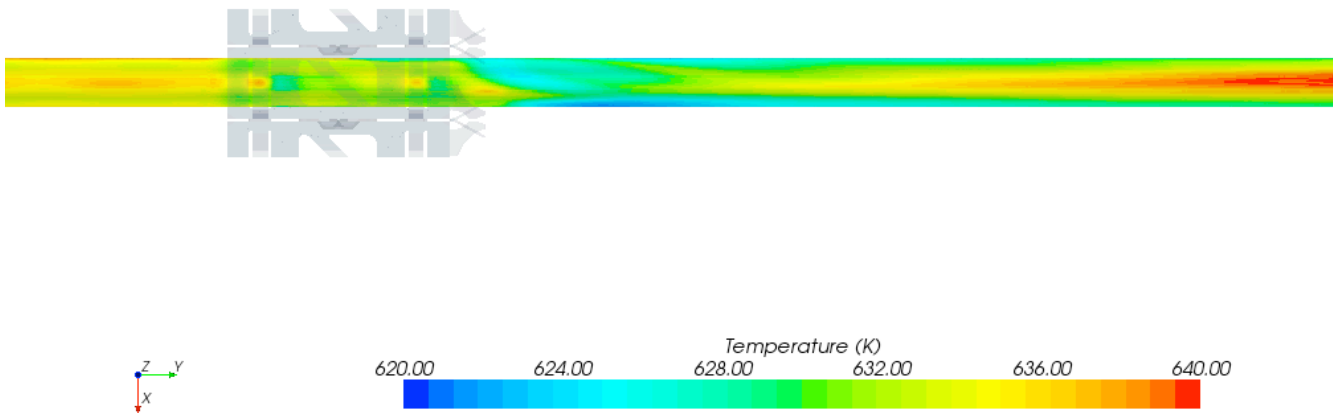


Figure 12 - Temperature distribution on the central fuel rod for average power

### 3.4.2 Couple DeCART Modelling Results

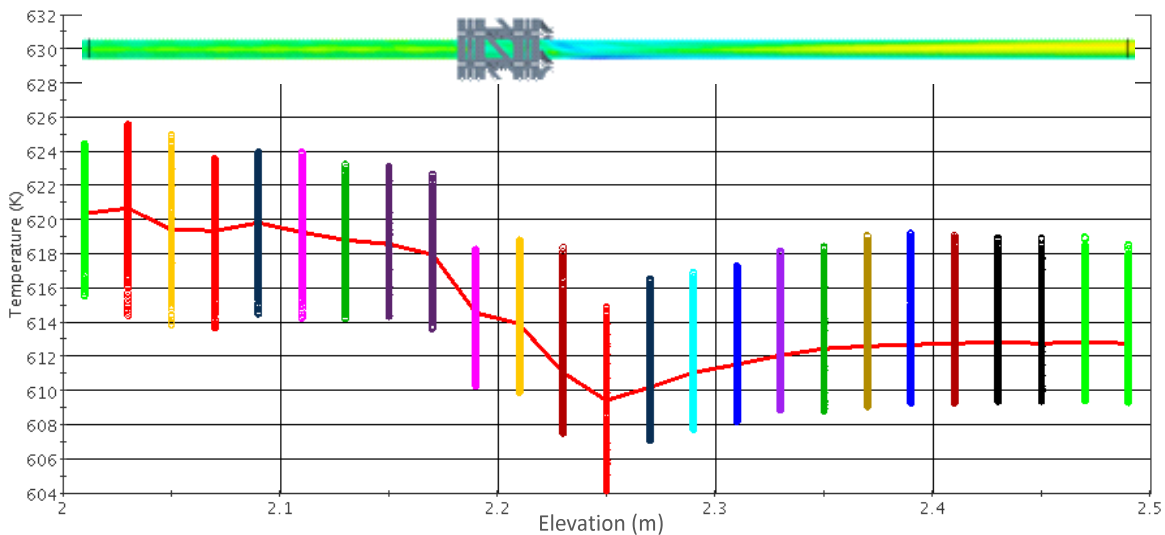


Figure 13 - Temperature distribution near the spacer grid on the central fuel rod from coupled model

As shown in Fig. 13, the results for the coupled case are very different. The temperature is much higher before the spacer but shows a much more relevant influence of the spacer grid. The high temperature before the spacer grid is caused by the axial power shift shown in Fig.6. Also this can be observed in the detailed distribution in Fig.14. The coolant temperature in Fig.15 shows cold spot at the channel center. After the spacer grid (50mm downstream), the cold spot has been moved near cladding by the mixing effect of the spacer grid. It is noticeable that the coolant temperature distribution is more even with the spacer grid. The spacer grid has clearly promoted the heat convection.

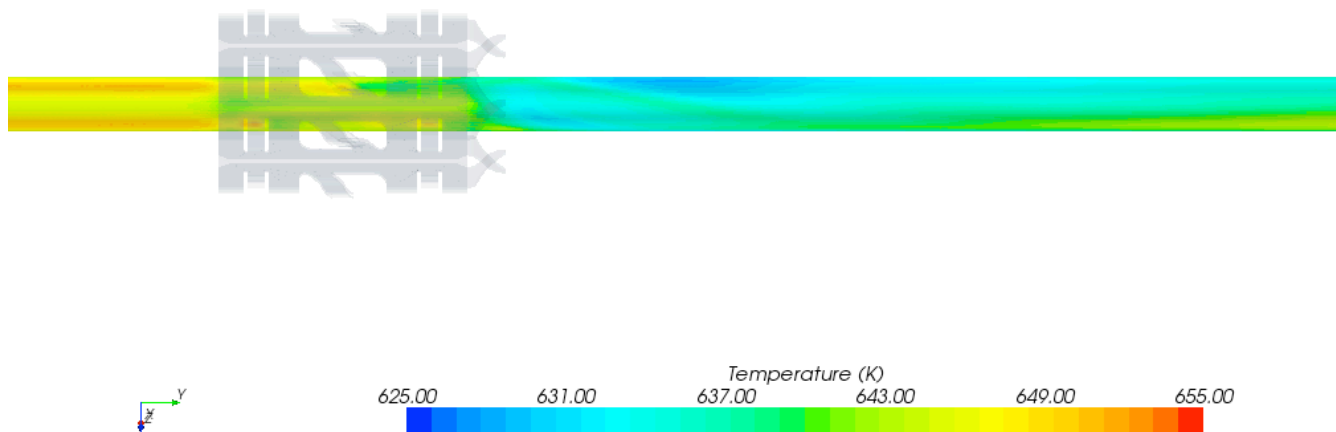


Figure 14 - Temperature distribution on the central fuel rod for coupled calculation

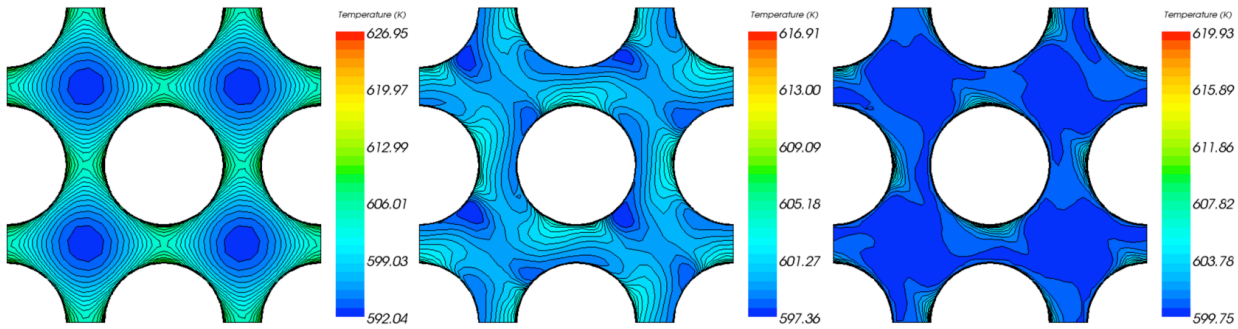


Figure 15 - Fluid Temperature Distribution 50mm upstream of the spacer, 50mm and 100mm downstream, the mixing is clearly noticeable (coupled flow case)

#### 4. Conclusion

This paper described coupled STAR-CCM+ / DeCART calculations for representative three-dimensional models with explicit representation of spacer grids with mixing vanes and the high fidelity results were compared to lower order simulations. The coupled CFD/MOC solution demonstrate the potential of the present approach to provide a more accurate model which includes a more truthful representation of all the important physics such as fission energy, heat convection, heat conduction, and turbulence. Of particular significance was the ability to assess the effects of the mixing grid on the coolant temperature and density distribution using coupled thermal/fluids and neutronic solutions. A more accurate cladding temperature was derived by this approach which will also enabled a better understanding of DNB margin and crud build up on the fuel rod. The CFD model gives results such as temperature, density, and velocity distribution inside the fuel pellet, cladding, and coolant. This 3X3 neutronic & CFD coupling model forms the base for the multi-physics 3X3 pin model. In the future, the corrosion model, the curd buildup model, the pellet cladding interaction model (PCI), and finite element model will be all added.

Work is ongoing to extend the models developed here to full three dimensional models of the entire fuel assembly and in the future to multi-assembly sub-core models.

#### 5. References

- [1] H.G. Joo, et al., "Methods and Performance of a Three-Dimensional Whole-Core Transport Code DeCART", Proc. PHYSOR 2004, Chicago, Illinois, April 25-29, (2004).
- [2] B. KOCHUNAS, M. HURSIN and T. DOWNAR, "DeCART-v2.05 Theory Manual", University of Michigan, (2009).
- [3] D.P. Weber, et. al., "High Fidelity LWR Analysis with the Numerical Nuclear Reactor", Nuclear Science and Engineering, 155, 395-408, (2007).
- [4] T. Sofu, et al., "Coupled BWR Calculations with the Numerical Nuclear Reactor Software System", Proc. of M&C + SNA, Monterey, California, April 15-19, (2007).
- [5] H. L. McClusky, M. V. Holloway, T. A. Conover, D. E. Beasley, M. E. Conner, and L. D. Smith III, "Mapping of the Lateral Flow Field in Typical Subchannels of a Support Grid with Vanes," Journal of Fluids Engineering, Trans. ASME, 125, pp.987-996 (2003).

- [6] B. Liu, M. B. Dzodzo, D. V. Paramonov, L. D. Smith, III, M. E. Conner, and M. Y. Young, "Application of CFD in the Design Process for PWR Spacer Grid Mixing Vanes," Proceedings of the 2004 International Meeting on LWR Fuel Performance, Orlando, Florida, September 19-22, 2004, Paper 1065 (2004).
- [7] Smith III, L.D., Conner, M.E., Liu, B., Dzodzo, M.B., Paramonov, D.V., Beasley, D.E., Langford, H.M., Holloway, M.V., 2002. "Benchmarking computational fluid dynamics for application to PWR fuel. In: Proceedings of the 10th International Conference on Nuclear Engineering, Arlington, Virginia, USA, April 14–18.
- [8] B. Liu, L. D. Smith, III, M. E. Conner, M. B. Dzodzo, D. V. Paramonov, Z. E. Karoutas, R. P. Knott, and M. Y. Young, "CFD Approach for Investigating Flow and Heat Transfer in PWR Fuel Assembly," Proceedings of 13th International Conference on Nuclear Engineering (ICONE13), Beijing, China, May 16-20, 2005, ICONE13-50924 (2005).
- [9] M. E. Conner, E. Baglietto, A. M. Elmahdia, "CFD methodology and validation for single-phase flow in PWR fuel assemblies" Nuclear Engineering and Design, Volume 240, Issue 9, September 2010, Pages 2088-2095 (2009)
- [10] T-H. Shih, W. W. Liou, A. Shabbir, Z. Yang, and J. Zhu, 1994. "A New k- Eddy Viscosity Model for High Reynolds Number Turbulent Flows -- Model Development and Validation", NASA TM 106721.